Formation and behaviour of macrovortices during a turbulent relaxation process in high-T_c superconductors

2005 J. Phys.: Condens. Matter 17 2723

(http://iopscience.iop.org/0953-8984/17/17/021)

INSTITUTE OF PHYSICS PUBLISHING JOURNAL OF PHYSICS: CONDENSED MATTER

J. Phys.: Condens. Matter **17** (2005) 2723–2732 doi:10.1088/0953-8984/17/17/021

Formation and behaviour of macrovortices during a turbulent relaxation process in high-T_c superconductors

M R Koblischka[1] **and T H Johansen**[2,3]

[1] FR Experimentalphysik, Universität des Saarlandes, PO Box 151150, D-66041 Saarbrücken, Germany
[2] Department of Physics, University of Oslo, Blindern, N-0316 Oslo, Norway
[3] Texas Center for Superconductivity and Advanced Materials, University of Houston, Houston, TX 77204-5002, USA

Received 14 December 2004, in final form 31 March 2005
Published 15 April 2005
Online at stacks.iop.org/JPhysCM/17/2723

Abstract

The time dependence of flux patterns obtained on an untwinned $YBa_2Cu_3O_{7-\delta}$ single crystal showing the 'meandering instability' is observed at $T = 65$ K using magneto-optical imaging. When applying a reversed external field to a remanent state, along the front of invading antiflux, macrovortices or droplets of flux are formed, and eventually separate from the flux front in a spiral-like motion. The time-dependent behaviour of these macrovortices is investigated in detail.

(Some figures in this article are in colour only in the electronic version)

1. Introduction

The critical state of a type-II superconductor is normally considered to be stable, or quasi-stable, once it has been formed. However, recent experiments [1–4] have shown that flux turbulence or macroturbulence can occur in a narrow temperature window provided the sample is in a magnetic state containing domains of vortices and antivortices. Applying a reversed field to a previously generated remanent state with trapped flux causes the formation of a domain boundary, or vortex annihilation zone, between the pinned flux and the newly entering antiflux. In the case of $YBa_2Cu_3O_{7-\delta}$ (YBCO) single crystals above a temperature of approximately 47 K, the annihilation zone shows unstable behaviour as the invading flux causes it to form irregular meandering patterns. This behaviour persists until an upper limit in temperature ($\approx$80 K) is reached; above this limit, the irregular patterns vanish and the flux front again becomes regular. In several magneto-optic experiments, such flux turbulence was demonstrated in various samples, including twinned YBCO single crystals [3], underdoped YBCO single crystals [5] and $NdBa_2Cu_3O_{7-\delta}$ (NdBCO) single crystals [5, 6]. Untwinned YBCO crystals were found to display an even more drastic effect, as along the front of penetrating antivortices,

so-called 'flux droplets' or 'macrovortices' are formed, which can eventually separate from the flux front and move in a spiral-like fashion until complete annihilation occurs. This flux droplet formation is unique to YBCO single crystals, and was not observed in NdBCO crystals [5, 6] with higher flux pinning forces [7]. In this case, at the very end of the turbulent process, a kind of flux clustering just before the final annihilation step may occur [5, 6].

The recent progress concerning the theoretical explanation of this instability of the critical state by Bass *et al* [8, 9], based on the released heat due to the annihilation process, and by Fisher *et al* [10, 11] regarding the effects of anisotropy on hydrodynamic flow, requires a more detailed analysis of the experimental data. As stated by Fisher *et al* [11], for a comparison of theory and experiment, a microscopic model of the vortex annihilation process needs to be constructed. However, the formation of the flux droplets or macrovortices in untwinned YBCO crystals is a phenomenon which is still not covered by the theoretical analysis. In contrast to turbulence observed in NdBCO single crystals with constantly increasing temperature which could also be observed as jumps in the magnetization in SQUID measurements [12], the appearance of the macrovortices could not be detected in a corresponding magnetic relaxation experiment. Therefore, the formation and subsequent annihilation of the macrovortices is an especially important process to investigate in greater detail. While the theoretical explanation of this behaviour is still lacking, it is important to compile all experimental data that shed light on this intriguing phenomenon.

Therefore, in this work we present a detailed time-dependent magneto-optical investigation of states with such complex flux distributions near the upper temperature limit of the instability. The purpose of this work is to compile all experimental data in order to enable a complete theoretical description of the phenomenon. The main focus here is on the time behaviour of the flux droplets ('turbulent relaxation') in subsequent experimental runs performed under the same conditions.

2. Experimental details

Using the magneto-optical (MO) visualization techniques [13] based on the Faraday effect, which combine a high spatial resolution with the unique possibility to observe dynamic processes [13, 14] in real time, a direct observation of flux motion can be realized. MO relaxation experiments were performed either with constant magnetic field [15] or in the dynamic case [16]. The field distributions are obtained by the rotation of the polarization plane of linearly polarized light which passes a magneto-optically active layer exposed to the magnetic field of the underlying superconductor. From flux-free regions the light is reflected without rotation and thus cannot pass the microscope analyser, which is set in a crossed position with respect to the polarizer. The images presented here are, therefore, maps of the z-component of the local magnetic field, B_z, and increasing brightness corresponds to increasing values of $|B_z|$. As the magneto-optical active layer, we use a Bi-doped YIG film with in-plane magnetization. The microscope provides a uniform light field and a heat filter ensures that the heat load on the sample is negligible. The images are recorded using a digital camera (1536×1024 pixels per frame) and subsequently transferred to a computer for processing.

Single crystals of $YBa_2Cu_3O_{7-\delta}$ were grown by a self-flux method in Y-stabilized ZrO_2 crucibles. The crystals have a transition temperature $T_c = 93$ K and a sharp transition width $\Delta T_c \leqslant 0.25$ K. The crystal studied is a platelet with thickness $d \approx 50$ μm. By applying uniaxial stress parallel to the plate at $T = 450\,^{\circ}$C, the crystal was completely detwinned. The detwinning was monitored in a polarization microscope allowing the application of an optimum amount of stress.

In the magneto-optical apparatus the sample was mounted on the cold finger of an optical helium flow cryostat [13, 17]. The sample was glued onto a copper holder using GE varnish, and the indicator film is laid directly on the sample surface. The magnetic field was applied perpendicular to the sample surface (i.e., along the c-axis) using a copper solenoid coil with a maximum field of ± 120 mT.

3. Results and discussion

Firstly, we take a look at sequences of MO images showing how the turbulent relaxation process evolves in time. All the images are obtained in a time period after $t = 0$, when suddenly a reversed field of constant value is applied to a remanent state containing trapped flux in the central part of the crystal. The initial remanent state was obtained by applying the maximum field our coil can produce. The observation temperature was $T = 65$ K, and the MO images are recorded in steps of 10 s.

Figure 1 shows flux patterns of the YBCO single crystal at a reverse applied field of -12 mT. The first image, taken at $t = 10$ s, shows that the meandering of the boundary between positive (remanent) flux in the centre, and negative (invading) flux is well developed. Note also that the flux distribution *within* the invading flux front is very inhomogeneous, in stark contrast to the behaviour at lower temperatures. The entire flux arrangement appears to be in 'fast motion'. With increasing time ($t = 20$ s), a number of macrovortices or flux droplets are formed along the annihilation zone. These are seen in the images as bright droplets representing localized regions of enhanced flux density—two of them are marked by arrows in the image taken at $t = 20$ s. They are all located along the invading flux front, where one can note that the flux density gradients are largest. Eventually, these droplets start to move, often in a spiral-like fashion as seen, e.g., at $t = 100$ and 110 s (as marked by arrows) at the upper invading flux front. Here, a comet tail behind the droplet can be seen, indicating that droplets perform an anticlockwise spiral motion, according to the direction of the current. In contrast, one observes at the lower front that a flux droplet moves similarly in a clockwise direction.

We note that even after $t = 60$ s (e), new droplets are formed at the lower flux front while the majority of droplets were created in the interval between 10 and 20 s. The images and the corresponding flux density profiles clearly indicate that the invading antivortices at the flux front are in fast motion as compared to the flux in the rest of the sample. During the whole relaxation experiment, lasting for 150 s, the annihilation zone moves towards the sample centre by about 100 μm. Furthermore, the flux density profiles show a considerable decrease of the flux density gradients perpendicular to the flux front. The formation of flux droplets some time after the application of a negative field appears to be correlated with the large gradients towards the annihilation zone. After a period of motion of the droplet, it is again attracted by the flux front.

In figure 2, we present the experiment with an applied negative field of -28 mT. With this larger applied field, the flux gradients of the invading vortices are clearer and steeper. At 10 s, the flux front shows an extreme meandering, and there are already two droplets with an increased flux density formed. At $t = 20$ s, many flux droplets are present at the steepest flux density gradients; three of them are marked by arrows.

Between 60 and 90 s, some of the droplets that appeared first have now vanished, but also some new ones were generated. In the image taken at $t = 100$ s, the presence of a 'comet tail' behind a flux droplet is indicated by an arrow. At times larger than 100 s, some flux droplets are still present in the sample, but their number is reducing. Along the d-lines [18] especially, all droplets have annihilated and only four of them remain until $t = 150$ s. It is also important to note that the relaxation creates more homogeneous flux domains as compared to the first

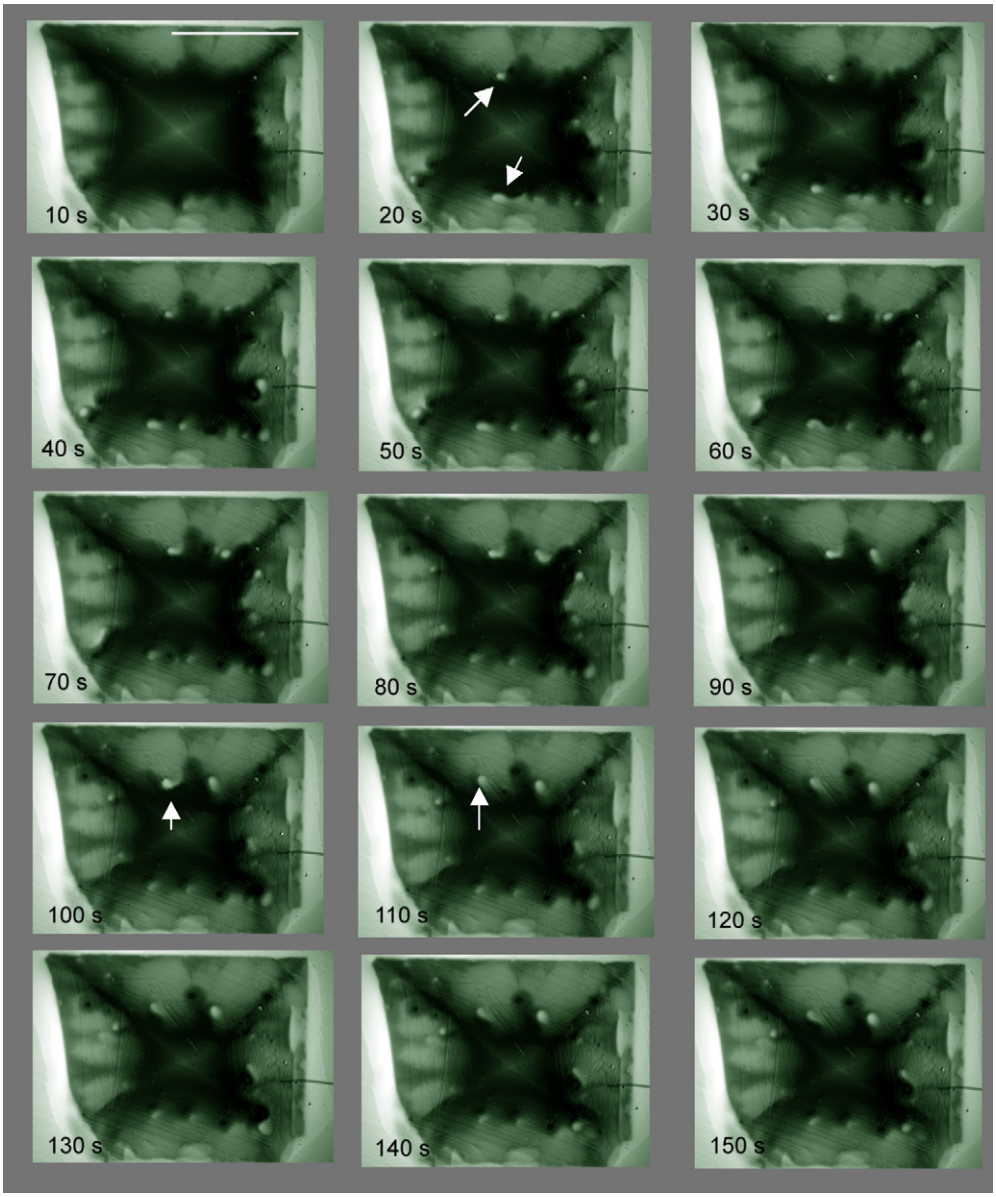

Figure 1. MO flux distributions observed on an untwinned YBCO single crystal at $T = 65$ K. The MO images are recorded in steps of 10 s, after a reversed field of -12 mT was applied to a remanent state obtained on applying +120 mT. During the experiment, this applied field is kept constant. It is clearly visible that the flux fronts do not exhibit a 'regular' shape, and flux droplets are formed at the steepest flux gradients, starting from the image taken at 20 s (marked by arrows). In the images at $t = 100$ and 110 s, the 'comet tail' behind a flux droplet is indicated by an arrow.

image at $t = 10$ s, especially along the invading flux front. On the right side of the sample, the flux front is found to enclose an area which persistently remains in the Meissner state. This situation is indicated in the image at $t = 120$ s by an arrow. The 2D graph of the flux distribution determined from the image at $t = 100$ s is presented in figure 3. In this graph,

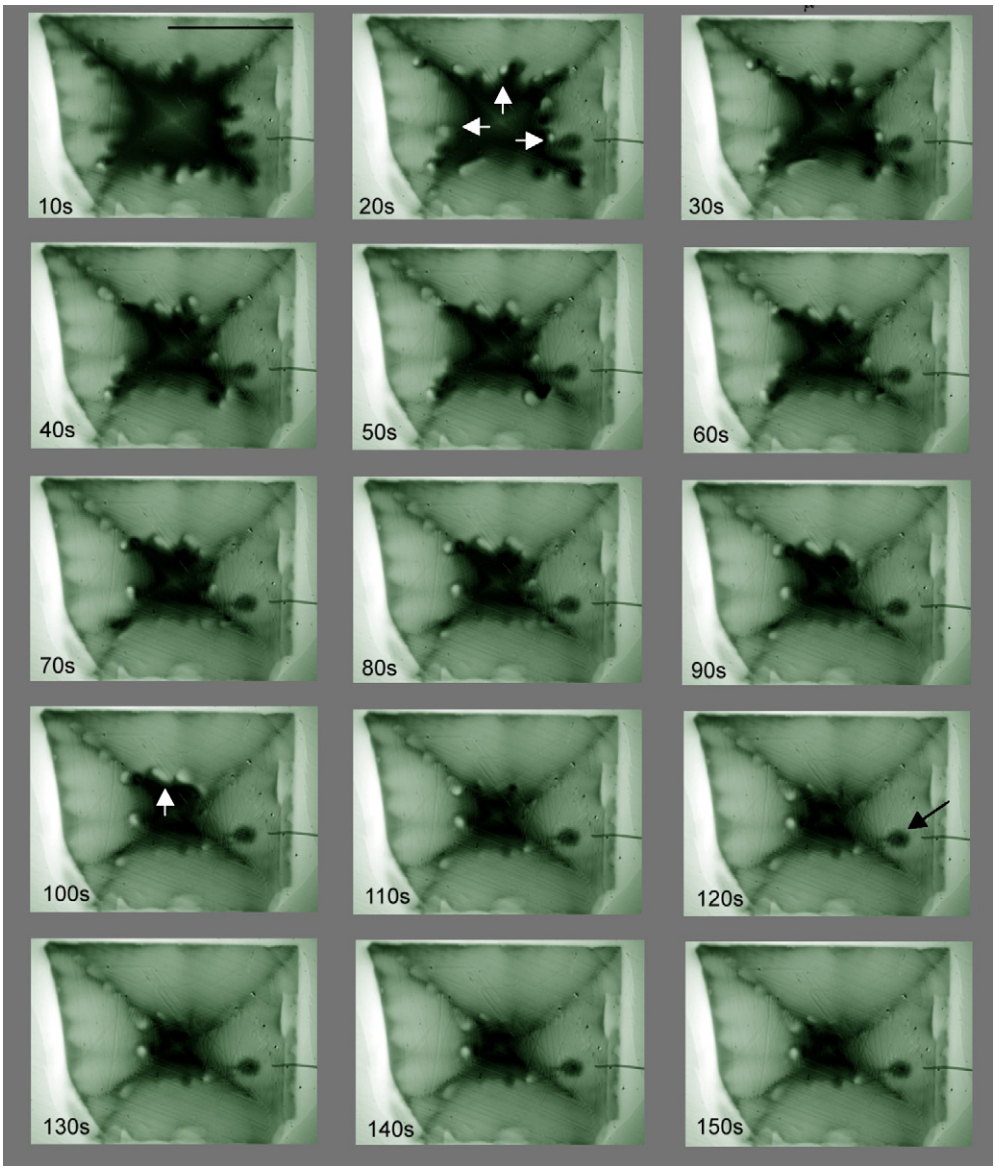

Figure 2. The same experiment as in figure 1, but with an applied negative field of −28 mT. With this larger applied field, the flux gradients of the invading vortices are clearer and steeper. The flux droplets are marked by arrows in the image taken at $t = 20$ s. At $t = 100$ s, a 'comet tail' behind a moving flux droplet is indicated by an arrow. At $t = 120$ s, a black arrow marks an area in the Meissner phase, which is completely enclosed by flux.

one can clearly see the field overshoot within the flux droplets as compared to the remainder of the flux front. Also the inner structure in the flux front at the left side becomes clearer.

Figure 4 presents another relaxation run with an applied negative field of −21 mT. Here, an uncrossed polarizer/analyser setting was used in order to enhance the MO contrast near the annihilation zone, as compared to a crossed setting which near $B = 0$ gives a low sensitivity parabolic Malus law contrast. Details of the influence of different polarizer settings were

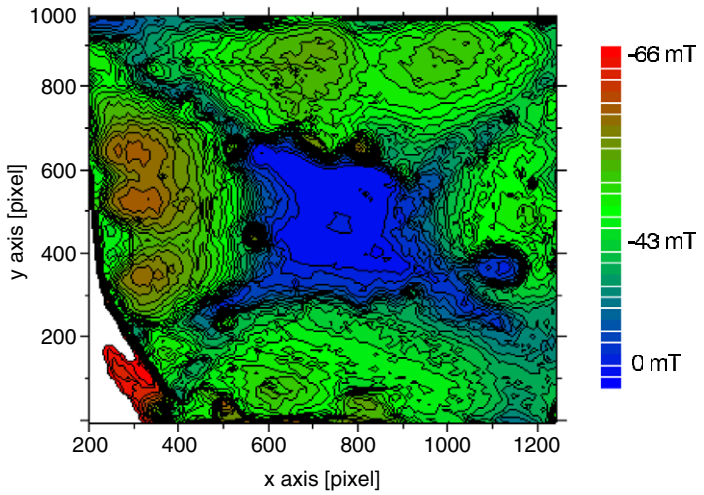

Figure 3. 2D plot of the flux distribution of the image at $t = 100$ s from figure 2. The field overshoot in a flux droplet is reaching -56 mT in an applied field of -28 mT.

discussed in [19]. In this setting it is, however, clearly visible that the flux droplets are formed in pairs; i.e., in both areas of flux and antiflux the droplets appear together. During their turbulent motion, the droplets move together and also annihilate again with each other.

For the further analysis of the relaxation process, we will now focus on details from figure 2. Figure 5 presents a series of difference images obtained by subtraction of two subsequent states in the early stages of the turbulent relaxation process shown in figure 2.

Image (a) is the difference between the images at $t = 10$ and 20 s, (b) the difference between 20 and 30 s, (c) the difference between 30 and 40 s, and (d) the difference between 40 and 50 s. In image (a), the formation of the flux droplets along the flux front becomes clearly visible. This process is accompanied by a considerable flux movement along the gradients within the invading domain towards the inside of the sample, but also *within* the flux front itself. This illustrates the visual impression that all the flux in the sample becomes 'fluid-like' during the instability. In (b), the movement of flux concentrates more towards the flux front, but still there is some movement inside the four invading domains. Images (c) and (d) illustrate that after a certain elapsed time, the flux movement takes place predominantly by the flux droplets.

From the experimental runs in applied fields between -12 and -28 mT, we analyse the statistical behaviour of the flux droplets. From several MO observations, it can be clearly seen that the flux droplets are formed where the flux density gradients are largest [18]; however, the location is never exactly reproduced in subsequent runs under the same conditions. The upper plot of figure 6 shows the number of droplets as a function of time, ranging between 0 and 200 s. The images of six independent experimental runs were recorded in intervals of 10 s. The open circles give the total number of droplets as a function of time. Here, we find that the majority of the droplets are produced about 20 s after turning on the reverse field. This zone of maximum activity stretches up to 50 s, and is followed by a minimum. A second maximum is then observed between 70 and 100 s. At later times, no new droplets are created any longer according to the decreasing flux density gradients due to the 'normal' relaxation process; however, it takes some extra time for all the droplets to disappear from the sample.

The lower plot in figure 6 presents an analysis of the time dependence of the maximum flux density within the droplets, using images from a single experimental run at an applied negative

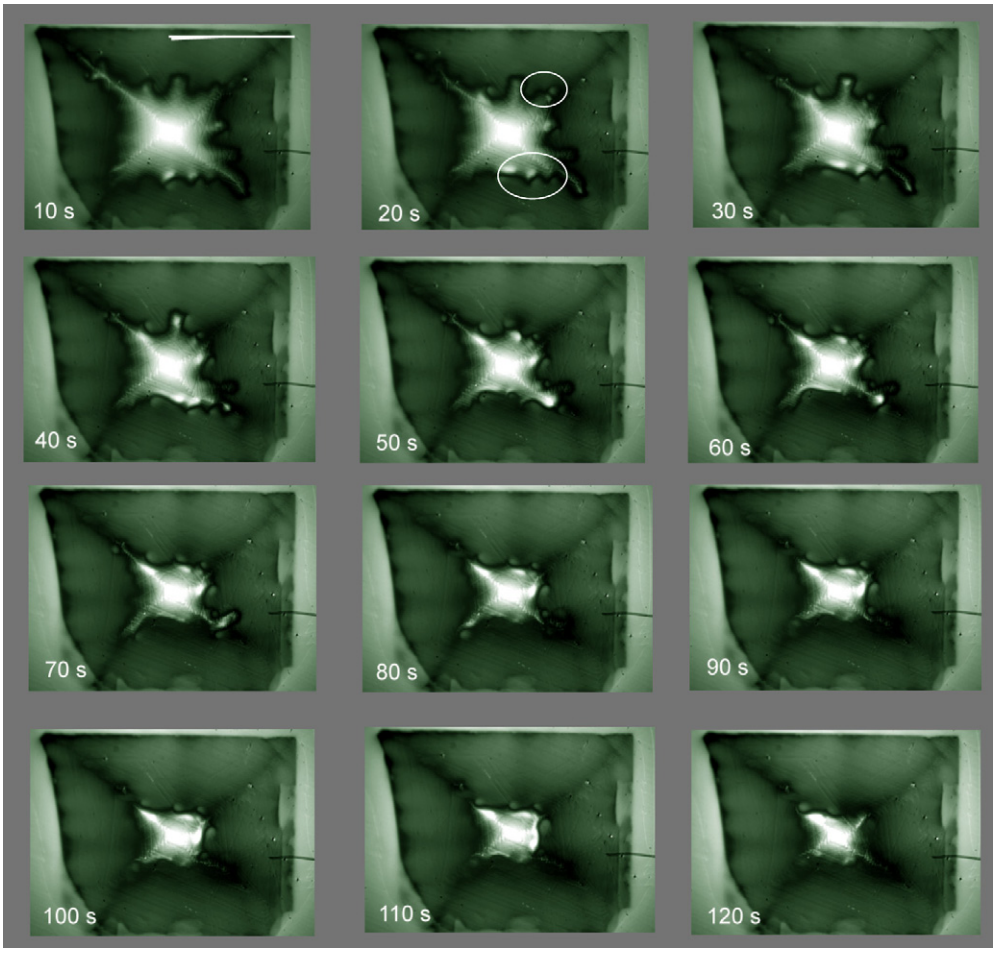

Figure 4. MO relaxation experiment with an applied negative field of −21 mT. In comparison to the previous experiments, a different polarizer setting is chosen so that the entering antiflux appears dark, while the remanent flux in the sample is appearing bright. In this configuration, we see that each flux droplet on the outer rim of flux is accompanied by another one on the side of the remanent flux. The two white circles in the image taken at $t = 20$ s indicate three such pairs of flux droplets.

field of −28 mT. Four droplets (1–4) were selected for this graph, each representing a different time behaviour. The extra line labelled 'flickering' illustrates the intensity differences due to the time variation of the microscope illumination, which is small enough to be disregarded. The graph clearly shows that there is a maximum flux density ($B_{z,\max}$) which a droplet can reach under 'normal' circumstances in comparison to the average B_z of the neighbouring flux front. The third run (Run 3) (△) shows another event: two droplets move towards each other and eventually merge together, thus forming a new much stronger droplet which reaches even $B_{z,\max} = -45$ mT, in spite the much lower applied field.

Such magneto-optic relaxation experiments were up to now only performed on detwinned YBCO single crystals [4] and on NdBCO single crystals [5]. These two types of sample are clearly distinguished by the very different critical current densities, which are considerably higher in the NdBCO system. Furthermore, the NdBCO crystals where turbulence was

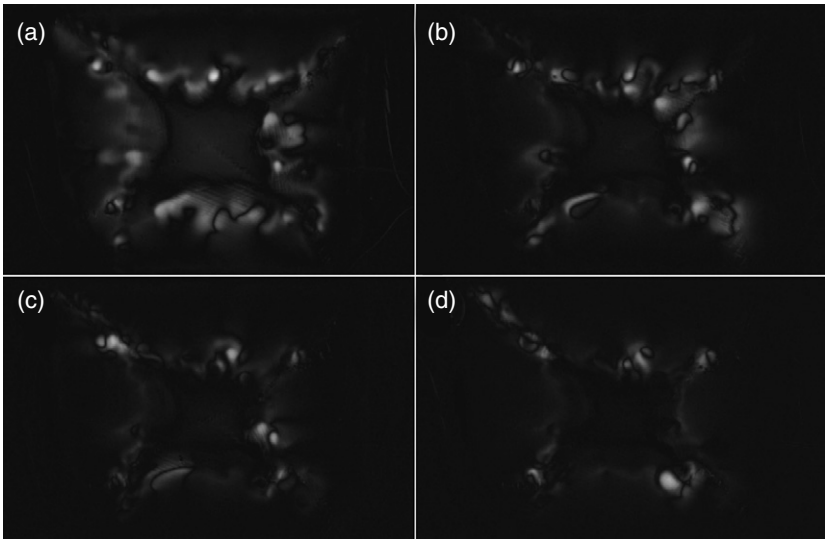

Figure 5. This figure presents a series of difference images obtained by subtraction of two subsequent states in the early stages of the turbulent relaxation process shown in figure 2. Image (a) is the difference between the images at $t = 10$ and 20 s, (b) the difference between 20 and 30 s, (c) the difference between 30 and 40 s, and (d) the difference between 40 and 50 s. In (a), the formation of the flux droplets along the ends of the flux fronts becomes clearly visible.

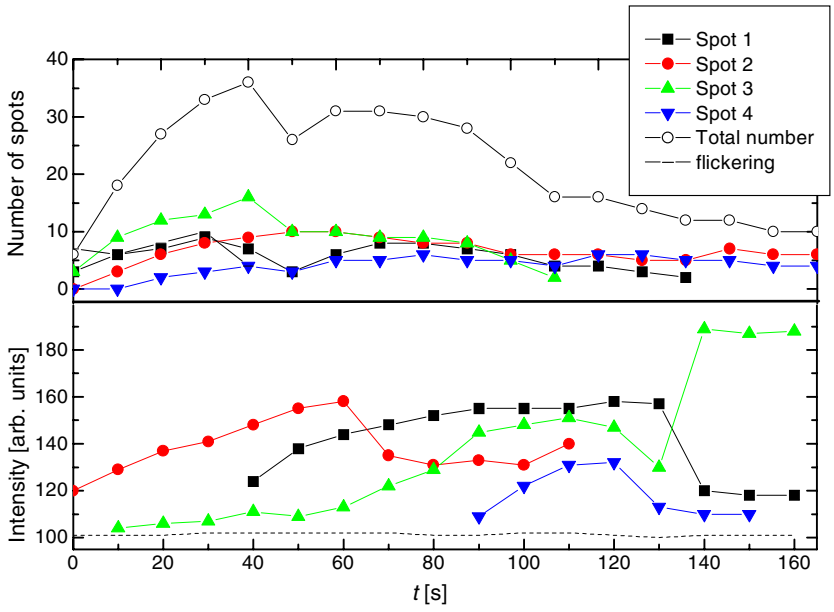

Figure 6. Analysis of the time dependence of the maximum flux density within the flux droplets, using images from a single experimental run at an applied negative field of −28 mT. Four droplets (1–4) were selected for this graph, each representing a different time behaviour. The extra line labelled 'flickering' illustrates the intensity differences due to the time instability of the microscope illumination, which is small enough to be disregarded.

observed, were heavily twinned. Twinned YBCO single crystals have never shown the formation of the flux droplets, so we may assume that the weaker flux pinning forces in the case of the untwinned single crystals are responsible for the formation of the flux droplets. Twinned YBCO samples, which were investigated for turbulence effects, did not present a clearly visible flux channelling as was observed earlier along differently oriented twin domains [13]. However, the anisotropy created by twins plays an important role in the theoretical explanation by Fisher *et al* [10, 11]. This implies that the small anisotropy of the critical currents within the (a, b)-plane may be enough to trigger the instability of the critical state. Another interesting observation is that in heavily twinned YBCO crystals the instability occurs at lower temperatures as compared to the untwinned YBCO single-crystal case studied here. On the other hand, in NdBCO single crystals, the turbulence occurs at much higher temperatures, which might be explained by the much higher flux pinning forces, assuming that the twinning (density and distance of the twins) and the (a, b)-anisotropy in NdBCO are similar to those of YBCO. Another important aspect is the fact that in melt-textured YBCO or NdBCO samples no turbulence effects have ever been observed [12]. The microstructure of these samples is mainly characterized by embedded Y_2BaCuO_5 particles and dense, criss-crossing twin boundaries, but the resulting flux pinning forces are only slightly higher as compared to those of corresponding single crystals [20]. Also this observation would favour an explanation of turbulence effects using a hydrodynamic approach.

In conclusion, we give a detailed presentation and analysis of the time dependence of the flux droplets formed during a turbulent relaxation process. These data should contribute to an extension of the recent theories to include this formation of droplets or macrovortices along the flux front.

Acknowledgments

We thank H Hauglin for providing the detwinned YBCO crystal. This work was financially supported by grant DAAD No. D/04/04403 and by the Norwegian Research Council, which is gratefully acknowledged.

References

[1] Indenbom M V, Schuster T, Koblischka M R, Forkl A, Kronmüller H, Dorosinskii L A, Vlasko-Vlasov V K, Polyanskii A A and Nikitenko V I 1993 *Physica* C **209** 259
[2] Johansen T H, Baziljevich M, Bratsberg H, Hauglin H and Lafyatis G P 1996 *High Temperature Superconductors: Synthesis, Processing, and Large-Scale Applications* ed U Balachandran, P J McGinn and J S Abell (New York: The Minerals, Metals, and Materials Society) p 203
[3] Vlasko-Vlasov V K, Nikitenko V I, Polyanskii A A, Crabtree G W, Welp U and Veal B W 1994 *Physica* C **222** 361
[4] Koblischka M R, Johansen T H, Baziljevich M, Hauglin H, Bratsberg H and Shapiro B Ya 1998 *Europhys. Lett.* **41** 419
[5] Frello T, Baziljevich M, Johansen T H, Andersen N H, Wolf Th and Koblischka M R 1999 *Phys. Rev.* B **59** R6639
[6] Koblischka M R, Murakami M, Koishikawa S, Johansen T H, Baziljevich M, Frello T and Wolf Th 1999 *J. Low Temp. Phys.* **117** 1483
[7] Koblischka M R, Higuchi T, Yoo S I and Murakami M 1998 *Phys. Rev.* B **58** 2683
[8] Bass F, Shapiro B Ya and Shvartser M 1998 *Phys. Rev. Lett.* **80** 2441
[9] Bass F, Shapiro B Ya, Shapiro I and Shvartser M 1998 *Phys. Rev.* B **58** 2878
[10] Fisher L M, Goa P E, Baziljevich M, Johansen T H, Rakhmanov A L and Yampolskii V A 2001 *Phys. Rev. Lett.* **87** 247005
[11] Fisher L M, Johansen T H, Rakhmanov A L, Levchenko A A and Yampolskii V A 2004 *Physica* C **403** 219

[12] Koblischka M R, Johansen T H, Baziljevich M and Murakami M 2002 *J. Supercond.* **15** 153
Koblischka M R, Koishikawa S and Murakami M 2000 *Physica* B **284–288** 785
Koblischka M R, Murakami M, Johansen T H, Baziljevich M, Frello T and Wolf Th 1999 *Phys. Status Solidi* b **215** R11
[13] Koblischka M R and Wijngaarden R J 1995 *Supercond. Sci. Technol.* **8** 199
[14] Hübener R P 1979 *Magnetic Flux Structures in Superconductors* (Berlin: Springer)
[15] Koblischka M R, Schuster Th, Ludescher B and Kronmüller H 1992 *Physica* C **190** 557
[16] Koblischka M R, Johansen T H, Bratsberg H, Půst L, Shen Y and Vase P 1997 *J. Phys.: Condens. Matter* **9** 10909
[17] Johansen T H, Baziljevich M, Bratsberg H, Galperin Y, Lindelof P E, Shen Y and Vase P 1996 *Phys. Rev.* B **54** 16264
[18] Schuster T, Indenbom M V, Koblischka M R, Kuhn H and Kronmüller H 1994 *Phys. Rev.* B **49** 3443
[19] Schuster Th, Koblischka M R, Kuhn M, Ludescher B, Leghissa M, Lippert M and Kronmüller H 1992 *Physica* C **196** 373
[20] van Dalen A J J, Koblischka M R, Kojo H, Sawada K, Higuchi T and Murakami M 1996 *Supercond. Sci. Technol.* **9** 659